




Microstructure and mechanical properties of the In–48Sn– x Ag low-temperature alloy

Duy Le Han^{1,2,3,*} , Yu-An Shen¹, Sanghun Jin², and Hiroshi Nishikawa¹

¹Department of Manufacturing Process, Joining and Welding Research Institute, Osaka University, 11-1 Mihogaoka, Ibaraki, Osaka 567-0047, Japan

²Graduate School of Engineering, Osaka University, 2-1 Yamadaoka, Suita, Osaka 565-0871, Japan

³Department of Welding Engineering and Metals Technology, School of Mechanical Engineering, Hanoi University of Science and Technology, No. 1 Dai Co Viet, Hai Ba Trung, Hanoi, Vietnam

Received: 10 February 2020

Accepted: 15 April 2020

Published online:

26 April 2020

© Springer Science+Business Media, LLC, part of Springer Nature 2020

ABSTRACT

Alloys with melting points < 150 °C are required for the development of flexible consumer devices. While the eutectic In–48Sn alloy is a promising candidate for these applications, its low tensile strength and low creep resistance during solid-state aging are of concern. The addition of Ag can address this issue to some extent; however, the effect of added Ag on the properties of the alloy is not well understood. Here, we studied the effects of added x Ag ($x = 0.5, 1.0, 1.5$ wt.%) on the fusion start temperature, microstructure, and mechanical properties of the In–Sn eutectic alloy and found that the fusion start temperature of the In–48Sn– x Ag alloy was reduced to around 113 °C due to the ternary eutectic reaction of In–Sn–Ag, in which ϵ -AgIn₂ only formed in the In–48Sn– x Ag alloys. In addition, smaller β -In₃Sn and γ -InSn₄ phases were produced through the formation of ϵ -AgIn₂, which affected the mechanical properties of the alloy. In–48Sn–1.5Ag, with the smallest grains, exhibited the highest tensile strength of 12.5 MPa via boundary strengthening. In–48Sn–1.5Ag fractured in transgranular mode, which is different from the intergranular fracturing of the eutectic alloy with relatively large grains. Conversely, In–48Sn–0.5Ag, with the highest soft- β -In₃Sn/hard- γ -InSn₄ ratio, showed the longest elongation of 64%, which is twice that of the eutectic In–48Sn alloy.

Introduction

Low-temperature alloys with melting points less than 150 °C are receiving increasing attention for the development of lighter and more cost-effective portable consumer devices with polymer substrates

[1–3]. Eutectic Sn–58Bi- and Sn–Bi-based alloys, with high tensile strength and suitable melting points, are commonly studied as low-temperature alloys [4–8]; however, they all exhibit brittleness after thermal aging because of the coarsened bismuth phase, which is a disadvantage [9]. In addition, their operating

Address correspondence to E-mail: hanleduy@jwri.osaka-u.ac.jp

temperatures exceed 160 °C [6, 7]. On the other hand, common flexible organic substrates, such as heat-stabilized polyethylene terephthalate (HS PET) and polyethylene naphthalate (PEN), require operating temperatures below 150 °C [10]; hence, these Sn–Bi alloys cannot be used with flexible organic substrates.

The eutectic In–48Sn alloy, with a melting point of 118 °C and good ductility and wetting behavior, is the most promising candidate for the above-mentioned low-temperature applications [11–13]. Nevertheless, low tensile strength and low creep resistance are critical concerns in an In–Sn-based alloy during solid-state aging [14, 15]. Some studies aimed at improving the mechanical properties of the In–Sn-based alloy by the addition of trace elements (Zn, Bi, and Ag) have been reported [16–18]. Among these, Sn–In alloys with added Ag not only exhibit enhanced elongation and creep resistance [15, 18, 19], but their lower electrical resistance has also been investigated [18]. However, these studies showed that amounts of Ag > 2.5% result in higher melting temperatures. Moreover, the effect of the amount of Ag in the eutectic In–Sn alloy on the tensile strength and melting point is important but is not yet well understood. To address this deficiency, in this study we investigated the fusion start temperatures, microstructures, and mechanical properties of In–48Sn–*x*Ag (ISA) alloys in which *x* = 0.5, 1.0, and 1.5 wt.%.

Materials and methods

Figure 1 presents a schematic of the experimental procedure. We fabricated ISA alloys consisting of commercial In–48Sn eutectic and 0.5, 1.0, and 1.5 wt.% Ag from pure silver wire (99.99%; Nilaco Corporation, Japan). These elements were alloyed at 700 °C for 5 h in an alumina crucible inside a furnace in a nitrogen atmosphere. The composition of the new alloys was analyzed as detailed below, the results of which are summarized in Table 1. Alloy bars (50 × 10 × 5 mm) were shaped using a casting mold, and then further shaped into dumbbells by wire electrical discharge machining (Sodick AG 360L, Japan). The dimensions of the dumbbells are shown in Fig. 1. Tensile testing was conducted under a strain rate of $5 \times 10^{-4} \text{ s}^{-1}$ using a universal tensile machine (Autograph AG-X, Shimadzu, Japan). The tensile elongation and ultimate tensile strength (UTS)

were determined from tensile stress–strain curves. The fracture surface of each tensile specimen was examined by scanning electron microscopy (SEM; SU-70, Hitachi, Japan).

The melting behavior of each ISA alloy was examined by differential scanning calorimetry (DSC; 7020 clinical analyzer, Hitachi, Japan) under a constant flow of N₂ in the range of 50–250 °C at a rate of approximately 10 °C/min. The fusion start temperature (*T_f*) was determined as required by the JIS Z 3198-1 standard. The microstructure of the ISAs was examined after grinding with SiC grit paper in the order #800, #1200, and #2000, and then successive polishing with 1.0 and 0.3 μm alumina suspension, respectively (Buehler, USA). The crystal structure of the ISA alloys was determined by X-ray diffraction (XRD; Ultima IV, Rigaku, Japan) in a range of 30°–80° 2θ at a scan rate of 1°/min. The microstructure and the elemental distribution of the ISAs was determined by SEM and field-emission electron-probe microanalysis (FE-EPMA; JXA-8530F JEOL). ImageJ software was used to calculate phase size and number.

Results and discussion

Melting behavior in relation to alloy phase constitution and microstructure

The DSC curves for all alloys are shown in Fig. 2a, from which the fusion start temperatures for the In–48Sn–0.5Ag (ISA4805), In–48Sn–1.0Ag (ISA4810), and In–48Sn–1.5Ag (ISA 4815) alloys were determined to be 112.6, 112.7, and 113.2 °C, respectively, which are all lower than that of the eutectic In–48Sn alloy (117.2 °C). The addition of Ag slightly decreases the fusion start temperature of eutectic In–48Sn, which is ascribable to the ternary eutectic reaction, and was calculated by Ohnuma et al. to be 114 °C for Sn–52.2In–0.9Ag (Eq. (1)). The melting temperature of Sn–51.7In with 1.0–5.0 wt.% added Ag was predicted to increase with increasing silver content [20], in agreement with the results in this study.



The XRD patterns for all alloys are displayed in Fig. 2b, which reveals the presence of ε-AgIn₂ in the new ISA alloys, as observed in other In–Sn–Ag alloys [19]. Although few studies have reported the

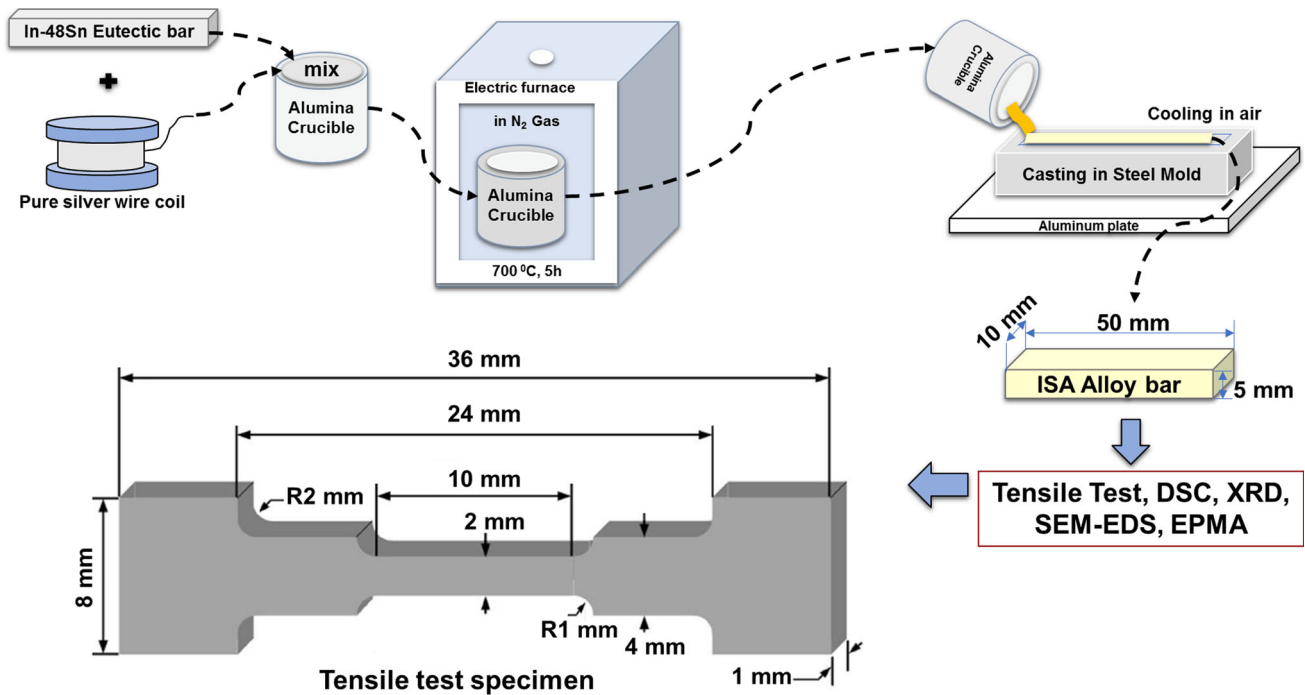


Figure 1 Schematic of the experimental procedure.

Table 1 Composition of the eutectic In–48Sn alloy and the In–48Sn–*x*Ag alloys

Alloy	In (wt.%)	Sn (wt.%)	Ag (wt.%)	Other (wt.%)
In–48Sn	52.08	47.91	–	0.01
In–48Sn–0.5Ag (ISA4805)	51.76	47.71	0.52	0.02
In–48Sn–1.0Ag (ISA4810)	51.11	47.84	1.00	0.05
In–48Sn–1.5Ag (ISA4815)	50.93	47.55	1.50	0.02

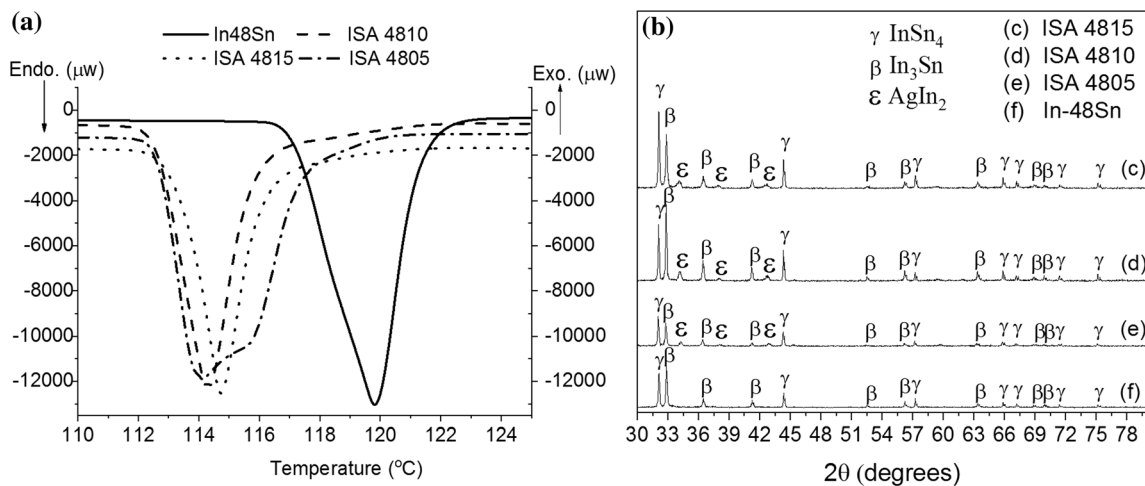


Figure 2 a DSC curves and b XRD patterns of the various alloys: In–48Sn, ISA4815, ISA4810, and ISA4805.

presence of the Ag_2In intermetallic compound (IMC) in ISA alloys [19, 21], Chuang et al. [22] reported that Ag_2In and $AgIn_2$ compete in In–49Sn/Ag alloyed

specimens during aging. At temperatures under $75\text{ }^\circ\text{C}$, the dominant reaction is:



Hence, the Ag-In IMC is transformed from Ag_2In to AgIn_2 , according to Eq. (2), in ISA alloys during slow cooling. In addition, EPMA maps of the alloys are shown in Fig. 3, with EPMA point analyses providing the elemental content of all phases, as summarized in Table 2. AgIn_2 , which is circular in shape, exists in the In_3Sn phase in the ISA alloys because the In-rich phase is required for transformation to occur, according to Eq. (2). The diameter of the AgIn_2 phase increases with the addition of more Ag, from 0.5–2.0 μm in the ISA 4805 and 4810 alloys to 2.0–4.0 μm in the ISA 4815 alloy, leading to a significant reduction in the $\gamma\text{-InSn}_4$ size. The microstructures of the eutectic In–48Sn and ISA alloys are displayed in Fig. 4a–d, which shows that the In-rich $\beta\text{-In}_3\text{Sn}$ appeared as dark regions, while the light areas correspond to $\gamma\text{-InSn}_4$ [14, 19]. We measured the area and number of phases, as summarized in Fig. 4e–g, which shows that the $\beta\text{-In}_3\text{Sn} + \varepsilon\text{-AgIn}_2$ phases in ISA4815 (135 μm^2) are smaller than $\beta\text{-In}_3\text{Sn}$ in eutectic In–48Sn (270 μm^2). Moreover, the $\gamma\text{-InSn}_4$ phase in eutectic In–48Sn is, on average, 215 μm^2 in size; ISA4805 and ISA4810 show similar γ -phases that are approximately 120 μm^2 in size, while the average $\gamma\text{-InSn}_4$ phase in ISA4815 was found to be 300% smaller (65 μm^2), as shown in Fig. 4f. The $\beta\text{-In}_3\text{Sn}/\gamma\text{-InSn}_4$ ratio and the total number of phases in each alloy are displayed in Fig. 4g. The size of grains or phases in alloys is usually determined by the number of nucleation sites during solidification. When Ag was added to the eutectic In–48Sn alloy, the $\varepsilon\text{-AgIn}_2$ formed along the phase boundaries created additional sites for nucleation during cooling. Therefore, the addition of Ag affects the size of the phases, and its effects on the mechanical properties of the ISA alloys need to be considered.

Mechanical properties of alloys

The tensile strength and elongation of the alloys are presented in Fig. 5, which reveals that eutectic In–48Sn and ISA4810 exhibit the same tensile strength of about 10.5 MPa, while ISA4805 exhibits a lower tensile strength of 9.3 MPa, and the ISA4815 alloy exhibits the highest tensile strength of 12.5 MPa, as shown in Fig. 5a. In addition, the elongation of the new alloys was improved due to the addition of Ag, as is clearly evident in Fig. 5b, which shows that the

ISA4805 alloy presents the greatest elongation of 64%, which is twice that of the eutectic In–48Sn alloy (32%), followed by ISA4810 (52%) and ISA4815 (46%). The new alloys exhibit higher elongation but lower tensile strength compared with the eutectic Sn–58Bi alloy, namely 37.5% and 48.0 MPa, respectively [5].

The microstructure of a metal has an essential effect on its mechanical properties. As the microstructure was observed to change in this study, we were concerned about the impact of any change on the mechanical properties of the resultant alloys. Figure 5 shows typical stress–strain curves and a fracture image for each alloy; the maximum stress point and maximum strain in each curve determine the tensile strength and elongation of the alloy, respectively. The stress–strain curve of In–48Sn is typical of the ductile mode, with little plastic deformation; the curve tends to bulge before significantly dropping, while the specimen shows a typical brittle mode with planar stress fractures on inclined planes. We note that the eutectic In–48Sn alloy exhibits moderately ductile fracturing [19] or semi-ductile behavior. Conversely, the ISA samples exhibit ductile behavior with superior strain; the curves transit smoothly and fall slightly with the extensional tailing, in agreement with their macroscopic fracture morphologies, in which ISA4805 shows extreme elongation, with the longest necking region, followed by the ISA4810 and ISA4815 alloys. This alloy behavior is consistent with the elongation values, as shown in Fig. 5b.

The tensile strength was improved by the addition of more than 1.0 wt.% Ag. In particular, the ISA4815 alloy exhibited the highest tensile strength of 12.5 MPa. Mechanical strength depends on the dislocation capacity during plastic deformation [23], and the dislocations that accumulate at grain or phase boundaries induce grain-boundary strengthening in metals [24]. Therefore, the tensile strength of ISA4815 may be enhanced by its significantly smaller phases, as shown in Fig. 4e, f.

Figure 6a, b present dislocation-density gradients in large and small grains. The grain boundary is weakened in a large grain when a considerable dislocation-density gradient exists between the grain interior and the grain boundary, as shown in Fig. 6a [23]. Intergranular fracturing usually occurs in crystals with larger grains, because dislocation accumulations propagate cracks at grain boundaries during tensile testing [24]. Conversely, as shown in Fig. 6b,

Figure 3 EPMA maps of the In-48Sn, ISA4805, ISA4810, and ISA4815 alloys and the locations of the EPMA points listed in Table 2.

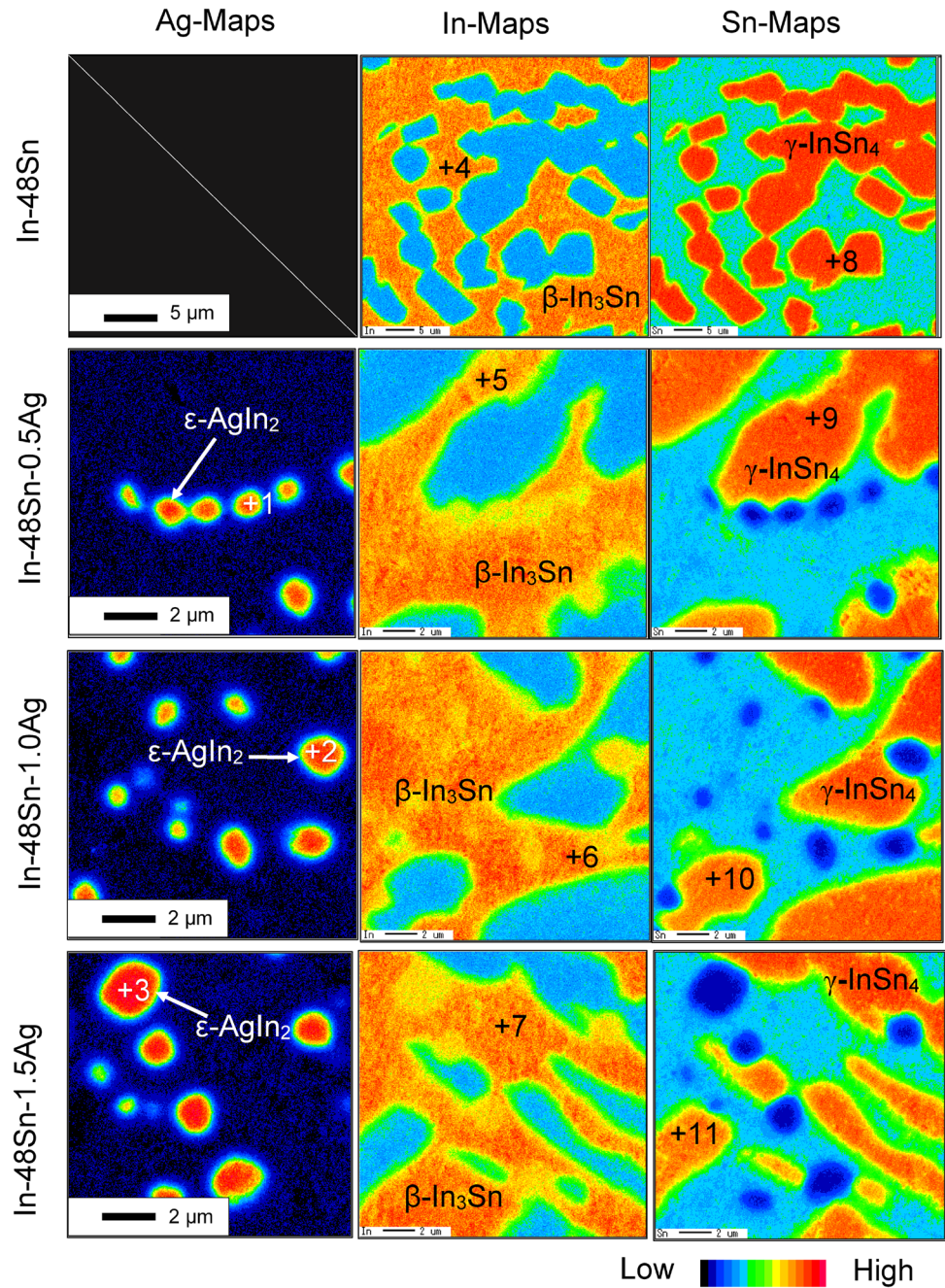


Table 2 Elemental composition of the points highlighted in Fig. 3

Points	Ag (at.%)	In (at.%)	Sn (at.%)	Proposed IMC
1–3	30.28–35.88	59.18–69.41	0.26–7.45	ϵ -AgIn ₂
4–7	0.02–1.71	74.82–77.16	22.81–23.47	β -In ₃ Sn
8–11	0.31–1.69	23.87–24.62	73.69–75.82	γ -InSn ₄

the grain boundaries are not the weakest regions during tensile testing in smaller grains with more uniform dislocation distributions, and transgranular

fracturing, as opposed to intergranular fracturing, is observed.

Fracture images following tensile testing are shown in Fig. 6c–f, with phases determined by energy-

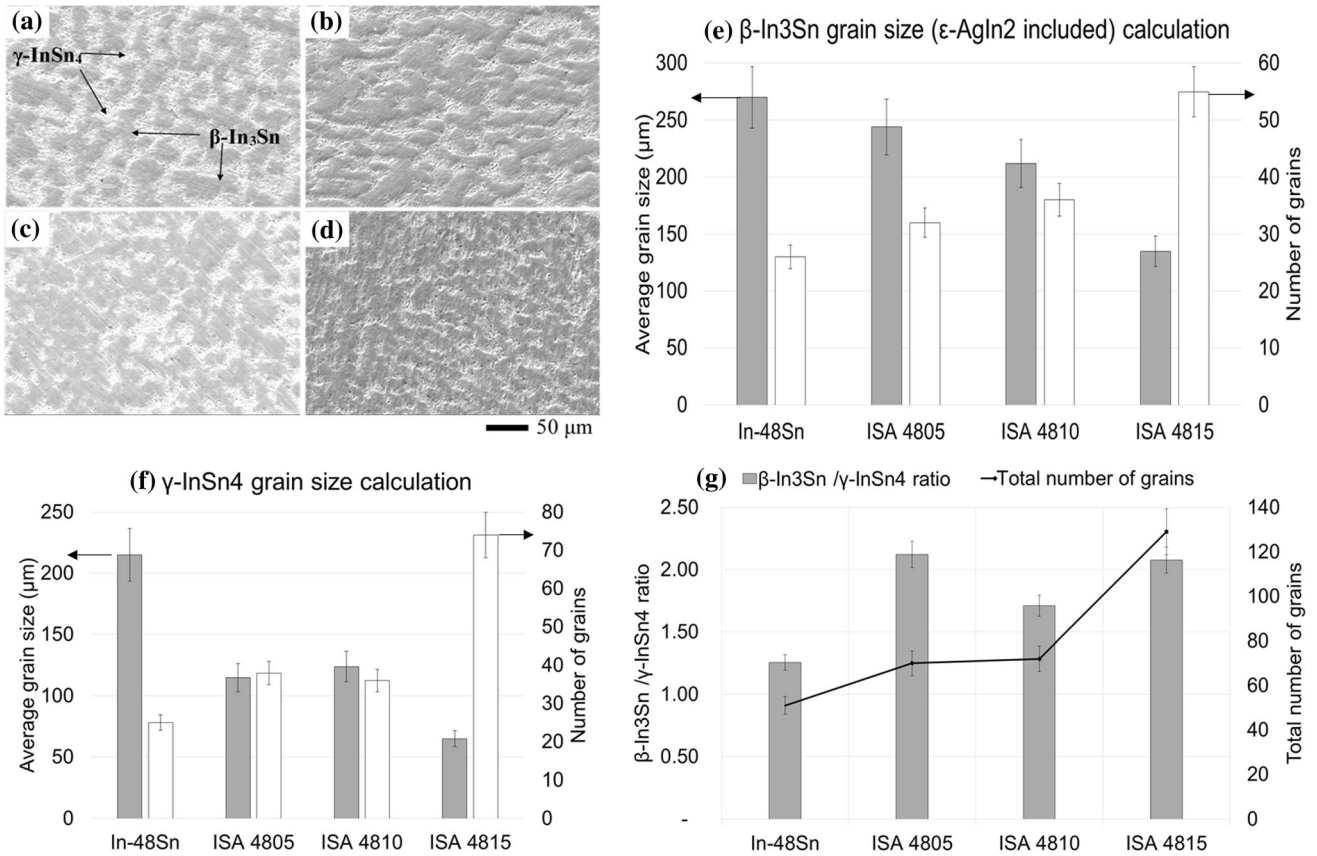
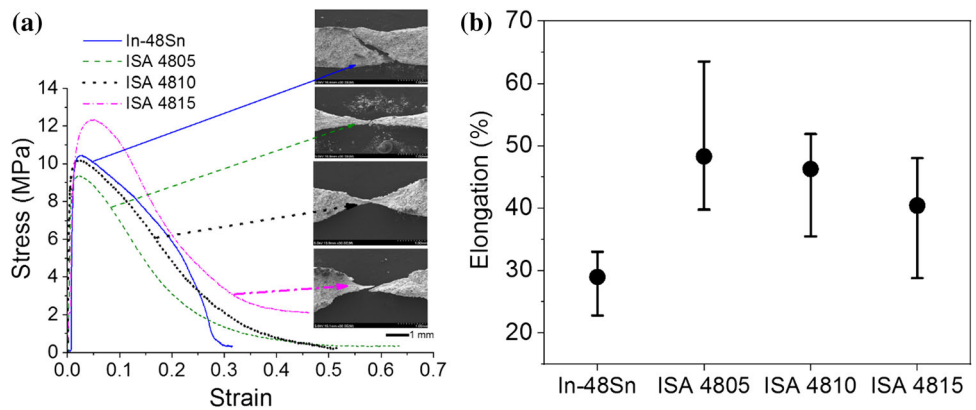


Figure 4 SEM images of various alloys ($\times 1000$ magnification): **a** In–48Sn, **b** In–48Sn–0.5Ag, **c** In–48Sn–1Ag, and **d** In–48Sn–1.5Ag; **e**, **f** grain calculation of the phases in each alloy; **g** β -In₃Sn/ γ -InSn₄ ratios and the total number of grains in each alloy.

Figure 5 a Representative stress–strain curves and fracture morphologies (SEM images) of various alloys; **b** elongation of the In-48Sn, ISA 4805, ISA 4810, and ISA 4815 alloys.

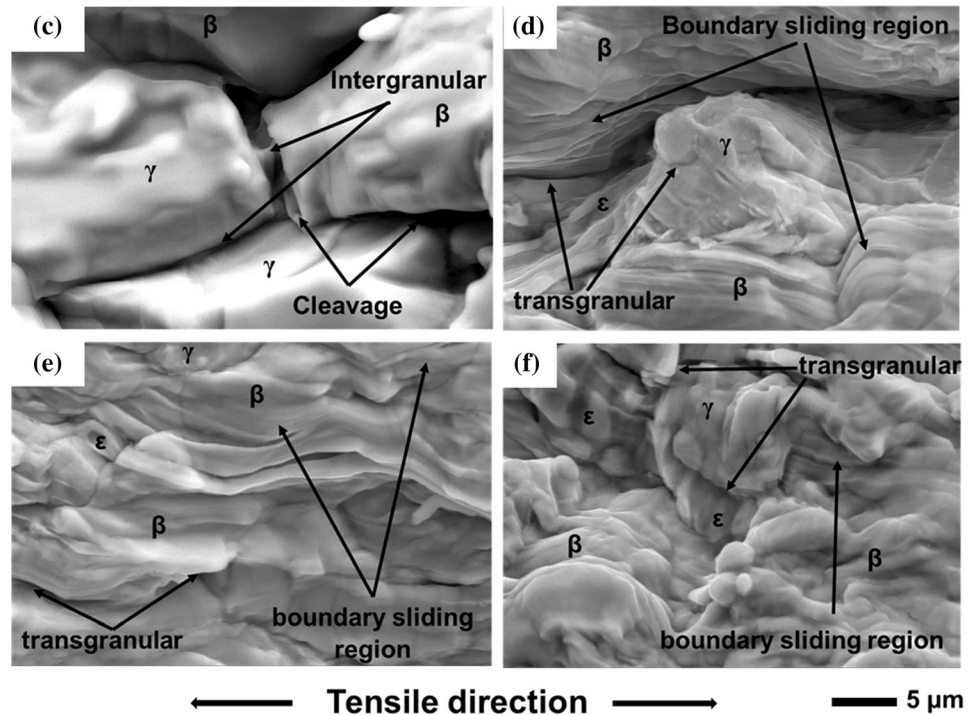
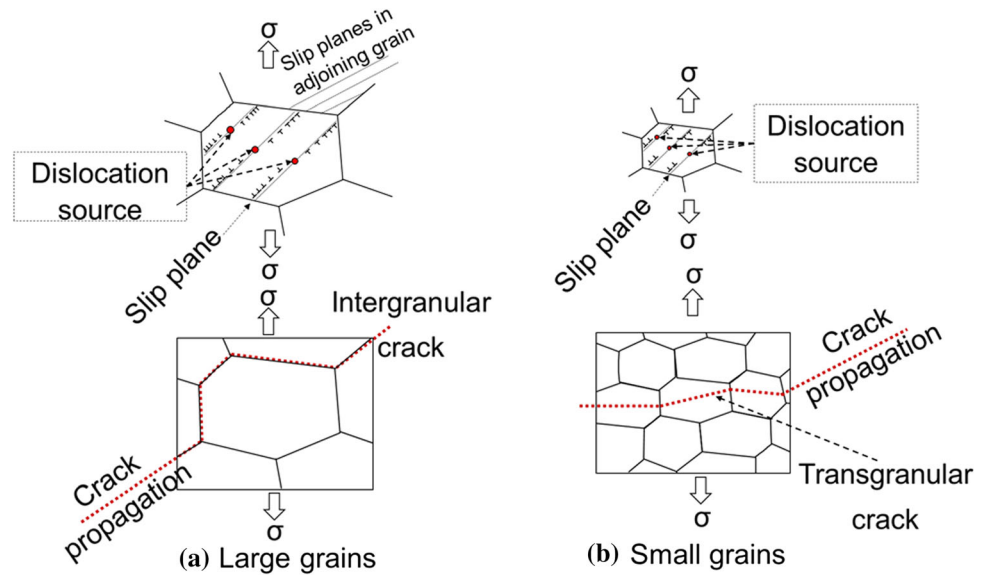


dispersive spectroscopy (EDS). Figure 6c reveals that the eutectic In–48Sn, with the largest phases, exhibits intergranular fracturing through cleavage along the grain boundaries. Each cracked grain is differently oriented to give a crystalline structure that resembles fractured rock candy [25]. The SEM images in Fig. 6d and e reveal that the phases in ISA4805 and ISA4810 are elongated through grain boundary sliding (GBS) motions along their tensile axes as well as cleavage

that leads to grain cracking inside the phase [23]. On the other hand, the ISA4815 alloy, with the largest number of small phases (Fig. 4), shows the most transgranular fractures, with collision areas (Fig. 6f) and the highest tensile strength, as shown in Fig. 5a.

From another point of view, the ISA samples all exhibit better elongation than the eutectic In–48Sn alloy. The γ -InSn₄ in the ISA4805 alloy, which is known to be a hard phase [14], experiences a

Figure 6 a, b Dislocation-density gradients in large and small grains; and fracture images of c In–48Sn, d ISA4805, e ISA4810, and f ISA4815 after tensile testing.



significant decrease in phase area (Fig. 4f), while the soft- β - In_3Sn phase [14] is slightly reduced in size (Fig. 4e), leading to the highest β - $\text{In}_3\text{Sn}/\gamma$ - InSn_4 ratio among the ISA alloys, as shown in Fig. 4g. On the other hand, the ISA4805 alloy, with the smallest Ag content, exhibits the lowest number of grains, while ISA4815, with the highest Ag content, shows the highest number of small grains among of the ISA alloys. In addition, as shown in the EPMA maps in Fig. 3, fewer hard γ - InSn_4 regions are observed in the

ISA alloys; the ϵ - AgIn_2 is formed in the β - In_3Sn phases due to the consumption of some of the In atoms, and near β - $\text{In}_3\text{Sn}/\gamma$ - InSn_4 phase boundaries. Although the β - In_3Sn regions in the ISA alloys include ϵ - AgIn_2 formations, hardness is largely dominated by the soft- β - In_3Sn phase. Accordingly, it is reasonable that ISA4805, with the highest β - $\text{In}_3\text{Sn}/\gamma$ - InSn_4 ratio and without a large number of small grains or phases for grain-boundary strengthening, is the softest among the alloys. Therefore, this study

reveals that the addition of Ag affects not only tensile strength, but also the elongation of the eutectic In–48Sn alloy.

Conclusions

In this study, eutectic In–48Sn was alloyed with 0.5–1.5 wt.% Ag to lower its fusion start temperature and enhance its mechanical properties. Due to the ternary eutectic reaction, the fusion start temperatures of the ISA alloys were all about 113 °C, which is lower than that of the eutectic In–48Sn alloy (117 °C). ε -AgIn₂ formed in β -In₃Sn phases and near β -In₃Sn/ γ -InSn₄ boundaries in the ISA alloys following the addition of Ag, which reduced the average areas of both β -In₃Sn phases and γ -InSn₄ phases; these smaller phases enhanced tensile strength and altered the fractured mode. ISA4815, with the smallest phases, was the strongest among the alloys, with a tensile strength of 12.5 MPa; this alloy fractured in transgranular mode, as commonly seen in crystals with small grains. In addition, all ISA alloys exhibited better elongation than the eutectic In–48Sn alloy, which is ascribable to smaller hard γ -InSn₄ regions. Among the alloys, ISA4805, with the highest soft- β -In₃Sn/hard- γ -InSn₄ ratio and devoid of very small phases, was the softest, with elongation of 64%. Therefore, the addition of Ag clearly influences the melting point, microstructures, tensile strength, and elongation of the eutectic In–48Sn alloy.

Acknowledgements

The authors wish to thank Dr. Shiqi Zhou for help and discussions during this research.

Compliance with ethical standards

Conflict of interest The authors declare that there are no conflicts of interest regarding the publication of this article.

References

- [1] Kim TW, Yan M, Erlat AG et al (2005) Transparent hybrid inorganic/organic barrier coatings for plastic organic light-emitting diode substrates. *J Vac Sci Technol A* 23:971–977. <https://doi.org/10.1116/1.1913680>
- [2] Liu YF, Feng J, Bi YG et al (2019) Recent developments in flexible organic light-emitting devices. *Adv Mater Technol* 4:1–19. <https://doi.org/10.1002/admt.201800371>
- [3] Shen Y-A, Zhou S, Li J et al (2019) Sn–3.0Ag–0.5Cu/Sn–58Bi composite solder joint assembled using a low-temperature reflow process for PoP technology. *Mater Des* 183:108144. <https://doi.org/10.1016/j.matdes.2019.108144>
- [4] Shen YA, Zhou S, Li J et al (2019) Thermomigration induced microstructure and property changes in Sn–58Bi solders. *Mater Des*. <https://doi.org/10.1016/j.matdes.2019.107619>
- [5] Zhou S, Shen YA, Uresti T et al (2019) Improved mechanical properties induced by In and In & Zn double additions to eutectic Sn58Bi alloy. *J Mater Sci: Mater Electron* 30:7423–7434. <https://doi.org/10.1007/s10854-019-01056-y>
- [6] Gleason J, Schroeder V, Henshall G et al (2008) Design, materials, and assembly process of high-density packages with a low-temperature lead-free solder (SnBiAg). *Solder Surf Mt Technol* 20(2):11–20. <https://doi.org/10.1108/09540910810871520>
- [7] Mei Z, Morris JW (1992) Characterization of eutectic Sn–Bi solder joints. *J Electron Mater* 21:599–607. <https://doi.org/10.1007/BF02655427>
- [8] Zhou S, Mokhtari O, Rafique MG et al (2018) Improvement in the mechanical properties of eutectic Sn58Bi alloy by 0.5 and 1 wt.% Zn addition before and after thermal aging. *J Alloys Compd* 765:1243–1252. <https://doi.org/10.1016/j.jallcom.2018.06.121>
- [9] Wang F, Chen H, Huang Y et al (2019) Recent progress on the development of Sn–Bi based low-temperature Pb-free solders. *J Mater Sci: Mater Electron* 30:3222–3243
- [10] Macdonald WA (2007) Latest advances in substrates for flexible electronics. *J Soc Inf Disp* 15:1075–1083. <https://doi.org/10.1889/1.2825093>
- [11] Chuang TH, Yu CL, Chang SY, Wang SS (2002) Phase identification and growth kinetics of the intermetallic compounds formed during In–49Sn/Cu soldering reactions. *J Electron Mater* 31:640–645. <https://doi.org/10.1007/s11664-002-0136-1>
- [12] Abteu M, Selvaduray G (2000) Lead-free solders in microelectronics. *Mater Sci Eng R Rep* 27:95–141. [https://doi.org/10.1016/S0927-796X\(00\)00010-3](https://doi.org/10.1016/S0927-796X(00)00010-3)
- [13] Kim SH, Yang S (2017) Low melting temperature solder materials for use in flexible microelectronic packaging applications. In: *Recent progress in soldering materials*. Intech, pp 8–37
- [14] Goldstein JLF, Morris JW (1994) The effect of substrate on microstructure and creep of eutectic In–Sn. *Metall Mater Trans Trans A* 323:2715–2722. <https://doi.org/10.1557/PR-OC-323-159>

- [15] Glazer J (1995) Metallurgy of low temperature Pb-free solders for electronic assembly. *Int Mater Rev* 40:65–93. <https://doi.org/10.1179/imr.1995.40.2.65>
- [16] Wang J, Mao D, Shi L et al (2019) Effect of zinc addition on the microstructure, thermal and mechanical properties of indium-Tin-xZinc alloys. *J Electron Mater* 48:817–826. <https://doi.org/10.1007/s11664-018-6768-6>
- [17] Kim SH, Yeon S-M, Kim JH et al (2019) Fine microstructured In–Sn–Bi solder for adhesion on a flexible PET substrate: its effect on superplasticity and toughness. *ACS Appl Mater Interfaces*. <https://doi.org/10.1021/acsami.9b04159>
- [18] El-Bediwi AB, El-Bahay MM (2004) Influence of silver on structural, electrical, mechanical and soldering properties of tin-indium based alloys. *Radiat Eff Defects Solids* 159:133–140. <https://doi.org/10.1080/10420150410001670288>
- [19] Jones WK, Liu Y, Shah M, Clarke R (1997) Mechanical properties of Pb/Sn Pb/In and Sn–In solders. *Solder Surf Mt Technol*, 37–41
- [20] Ohnuma I, Cui Y, Liu XJ et al (2000) Phase equilibria of Sn–In based micro-soldering alloys. *J Electron Mater* 29:1113–1121. <https://doi.org/10.1007/s11664-000-0002-y>
- [21] Korhonen TM, Kivilahti JK (1998) Thermodynamics of the Sn–In–Ag solder system. *J Electron Mater* 27:149–158. <https://doi.org/10.1007/s11664-998-0205-1>
- [22] Chuang TH, Huang YT, Tsao LC (2001) AgIn₂/Ag₂In transformations in an In–49Sn/Ag soldered joint under thermal aging. *J Electron Mater* 30:945–950
- [23] Callister WD Jr, Rethwisch DG (2015) *Fundamentals materials science and engineering: an integrated approach*, 5th edn. Wiley, London
- [24] Lu K, Lu L, Suresh S (2009) Strengthening materials by boundaries at the nanoscale. *Science* 80:349–353. <https://doi.org/10.1126/science.1159610>
- [25] Askeland DR, Fulay PP (2009) *Essentials of materials science and engineering*, second. Cengage Learning, Toronto ON M1K 5G4 Canada

Publisher's Note Springer Nature remains neutral with regard to jurisdictional claims in published maps and institutional affiliations.